1 # Regional Influence of Wildfires on Aerosol Chemistry in the
2 # Western US and Insights into Atmospheric Aging of Biomass
3 # Burning Organic Aerosol

4 Shan Zhou[1], Sonya Collier[1], Daniel A. Jaffe[2,3], Nicole L. Briggs[2,3,4], Jonathan Hee[2,3], Arthur J.
5 Sedlacek III[5], Lawrence Kleinman[5], Timothy B. Onasch[6], Qi Zhang[1*]

6 [1]Department of Environmental Toxicology, University of California, Davis, CA 95616, USA
7 [2]School of Science, Technology, Engineering, and Mathematics, University of Washington Bothell, Bothell, WA
8 98011, USA
9 [3]Department of Atmospheric Sciences, University of Washington, Seattle, WA 98195, USA
10 [4]Gradient, Seattle, WA 98101, USA
11 [5]Environmental and Climate Sciences Department, Brookhaven National Laboratory, Upton, NY 11973, USA
12 [6]Aerodyne Research Inc., Billerica, MA 01821, USA
13
14 *Corresponding Author: Qi Zhang (dkwzhang@ucdavis.edu), (530)752-5779, Department of Environmental
15 Toxicology, University of California, Davis, CA 95616

16 In preparation for Atmospheric Chemistry and Physics

17 Abstract. Biomass burning (BB) is one of the most important contributors to atmospheric aerosols on a global scale
18 and wildfires are a large source of emissions that impact regional air quality and global climate. As part of the
19 Biomass Burning Observation Project (BBOP) field campaign in summer 2013, we deployed a High Resolution
20 Time-of-Flight Aerosol Mass Spectrometer (HR-AMS) coupled with a thermodenuder at the Mt. Bachelor
21 Observatory (MBO, ~2.8 km above sea level) to characterize the impact of wildfire emissions on aerosol loading
22 and properties in the Pacific Northwest region of the United States. MBO represents a remote background site in the
23 western U.S. and it is frequently influenced by transported wildfire plumes during summer. Very clean conditions
24 were observed at this site during periods without BB influence where the 5-min average ($\pm$ 1σ) concentration of
25 non-refractory submicron aerosols (NR-PM$_1$) was 3.7 ± 4.2 μg m^{-3}. Aerosol concentration increased substantially
26 (reaching up to 210 μg m^{-3} of NR-PM$_1$) for periods impacted by transported BB plumes and aerosol composition
27 was overwhelmingly organic. Based on Positive Matrix Factorization (PMF) of the HR-AMS data, three types of
28 BB organic aerosol (BBOA) were identified, including a fresh, semivolatile BBOA-1 (O/C = 0.35; 20% of OA mass)
29 that correlated well with ammonium nitrate, an intermediately oxidized BBOA-2 (O/C = 0.60; 17% of OA mass),
30 and a highly oxidized BBOA-3 (O/C = 1.06; 31% of OA mass) that showed very low volatility with only ~ 40%
31 mass loss at 200°C. The remaining 32% of the organic aerosol (OA) mass was attributed to a boundary layer (BL)
32 OOA (BL-OOA; O/C = 0.69) representing OA influenced by BL dynamics and a low-volatility oxygenated OA
33 (LV-OOA; O/C = 1.09) representing regional free troposphere aerosol. The mass spectrum of BBOA-3 resembled
34 that of LV-OOA and had negligible contributions from the HR-AMS BB tracer ions – C$_2$H$_4$O$_2^+$ (m/z = 60.021) and
35 C$_3$H$_5$O$_2^+$ (m/z = 73.029). This finding highlights the possibility that the influence of BB emission could be
36 underestimated in regional air masses where highly oxidized BBOA (e.g. BBOA-3) might be a significant aerosol

Atmospheric
Chemistry
and Physics
Discussions

Open Access

EGU

37 component. We also examined OA chemical evolution for persistent BB plume events originating from a single fire

38 source and found that longer solar radiation led to higher mass fraction of the chemically aged BBOA-2 and BBOA-

39 3 and more oxidized aerosol. However, an analysis of the enhancement ratios of OA relative to CO (ΔOA/ΔCO)

40 showed little difference between BB plumes transported primarily at night versus during the day, despite evidence of

41 substantial chemical transformation in OA induced by photo-oxidation. These results indicate negligible net OA

42 production with photo-oxidation for wildfire plumes observed in this study, for which a possible reason is that SOA

43 formation was almost entirely balanced by BBOA volatilization.

44 **1   Introduction**

45   Biomass burning (BB) is estimated to be the largest source of primary carbonaceous aerosols and a major source

46 of reactive trace gases in the Earth's atmosphere (Bond et al., 2004; Akagi et al., 2011). Emissions from wildfires

47 and other BB sources, such as residential wood combustion and agricultural burning, have been shown to affect the

48 global radiation budget (IPCC, 2013) and degrade air quality in both rural areas and populated locations (e.g. Jaffe et

49 al., 2008; Jaffe and Wigder, 2012). The environmental impacts of BB emissions are strongly correlated with the

50 chemical, optical, and microphysical properties of BB aerosols, which are in turn dependent in a complex manner on

51 fuel type, combustion phase, and atmospheric aging of emitted particles and gas species (e.g., Petters et al., 2009;

52 Liu et al., 2014; Collier et al., 2016).

53   Organic compounds are a dominant component of BB aerosols (Bond et al., 2004; De Gouw and Jimenez, 2009),

54 but the chemical and physical properties of primary organic aerosol (POA) released directly from burning and

55 secondary organic aerosol (SOA) formed from gaseous precursors emitted by BB are dramatically different. For

56 example, BB POA tends to be semivolatile, smaller in size, and composed of less oxidized compounds, whereas

57 SOA from BB is generally more oxidized, larger in size, and less volatile (Abel et al., 2003; Heringa et al., 2011;

58 May et al., 2013). Furthermore, aerosol composition, optical properties, and hygroscopicity have been found to

59 change substantially in BB plumes undergoing photo-oxidation and cloud processing and the changes are mostly

60 driven by the organic fraction (Abel et al., 2003; de Gouw et al., 2006; Engelhart et al., 2012). Understanding the

61 chemical properties and atmospheric processing of organic aerosols (OA) from BB sources (i.e., BBOA) is thus

62 crucial for improving our ability to quantitatively assess and predict the impacts of BB emissions on climate and air

63 quality. However, the chemical processing of BBOA is highly complex and the net effect of aging on BBOA mass is

64 highly variable. For example, while several laboratory studies reported substantial formation of SOA during

65 chamber aging, others observed a very small increase or even a decrease of BBOA mass (Grieshop et al., 2009;

66 Cubison et al., 2011; Hennigan et al., 2011; Heringa et al., 2011; Ortega et al., 2013). Field studies have also

67 observed enhancement (Yokelson et al., 2009; DeCarlo et al., 2010), depletion (e.g.,Akagi et al., 2012; Jolleys et al.,

68 2015), or no change (Brito et al., 2014; May et al., 2015) of dilution-adjusted OA mass in BB plumes after emissions.

69   In order to decipher which factors affect BBOA evolution and reconcile discrepancies in previous laboratory and

70 atmospheric observational results, the U.S. Department of Energy (DOE) sponsored the Biomass Burning

71 Observation Project (BBOP) campaign, which combined aircraft-based measurements with mountain top

72 observations to characterize the downstream evolution of the chemical, microphysical, and optical properties of

Atmospheric
Chemistry
and Physics
Discussions

73   carbonaceous aerosol generated by BB. Wildfires across the western U.S. have been linked to increased $PM_{2.5}$

74   concentrations at various receptor sites (Jaffe et al., 2008) and high pollution episodes that exceeded the National

75   Ambient Air Quality Standards (Jaffe and Wigder, 2012). Furthermore, due to changes in precipitation, temperature

76   and other meteorological conditions as a result of climate change, wildfire activities in this region have been

77   increasing (Westerling et al., 2006; Dennison et al., 2014) and are predicted to increase summertime OA

78   concentration by 40% from 2000 - 2050 (Spracklen et al., 2009).

79   A large number of wildfire events originating in the western US were observed during BBOP from the Mount

80   Bachelor Observatory (MBO) – a remote mountain-top site that serves to characterize western U.S. background

81   conditions and is frequently impacted by transported BB plumes during the summer fire season (Wigder et al., 2013).

82   Continuous measurements of BB plumes at MBO allowed for the study of BBOA with different source, age, and

83   formation pathways under realistic atmospheric conditions and can provide rich data for evaluating the impact of BB

84   emissions on regional aerosol chemistry and elucidating their atmospheric aging processes. A number of recent

85   studies conducted at fixed locations in the western U.S. investigated impacts of BB on ozone, gaseous nitrogen

86   species, and organic and elemental carbon (e.g.,Wigder et al., 2013; Timonen et al., 2014; Hallar et al., 2015). Yet,

87   only a few ground-based measurements have examined the chemical composition and evolution of BBOA, including

88   a filter-based study of wildfire aerosols in Yosemite National Park (Engling et al., 2006) and a single-particle mass

89   spectrometry study on the mixing state and aging of particles during the 2007 San Diego wildfires (Zauscher et al.,

90   2013).

91   In this study, we provide an overview of the chemical and physical characteristics of non-refractory

92   submicrometer particles (NR-PM_1) at MBO and examine the changes in ambient aerosol concentration and

93   composition influenced by BB emissions. The sources of OA are investigated via factor analysis of the HR-AMS

94   data and the aging of BBOA are discussed via combining real-time measurements with trajectory analysis. We also

95   examine the enhancement and chemical transformation of OA in BB plumes transported during day-time and night-

96   time, respectively.

97   **2   Experimental methods**

98   **2.1   Sampling site and wildfires in the vicinity**

99   The Mt. Bachelor Observatory (43.981°N 121.691°W, Fig. 1) is situated on the summit of Mt. Bachelor (~ 2.8

100   km a.s.l.), an isolated volcanic peak in the Deschutes National (coniferous) Forest in central Oregon. The nearest

101   populated areas are Bend (pop. ~80,000), 31 km to the east, and Redmond (pop. ~ 26,000), 53 km northeast of MBO.

102   Due to its high elevation and distance from local pollution sources, MBO is a remote background site in the western

103   U.S. well positioned for sampling of background free tropospheric air and observation of long-range transport of

104   Asian plumes and North American wildfires (Weiss-Penzias et al., 2006; Wigder et al., 2013; Briggs et al., 2016).

105   During the sampling period from July 25 to August 25, 2013, various active wildfires in northern California and

106   southeastern and central Oregon were detected by the Moderate Resolution Imaging Spectroradiometer (MODIS)

107   satellite (https://firms.modaps.eosdis.nasa.gov) (Fig. 1). Three intense fires, the Salmon River Complex Fire (SRCF),

Atmospheric
Chemistry
and Physics
Discussions

108   Whiskey Complex Fire (WCF) and Douglas Complex Fire (DCF), were active for a majority of the time during this

109   study and hence were identified as major fires in the region.

110   **2.2   Real-time measurements at MBO**

111   Continuous observations at MBO included submicron aerosol light scattering (TSI nephelometer; 450, 550, and

112   700 nm) and absorption (Radiance Research PSAP; 467, 530, and 660 nm), elemental and organic carbon (Sunset

113   Lab), CO and CO_2 (Picarro Cavity Ring-Down Spectroscopy), O_3 (Dasibi), NO_x (Air Quality Design 2-channel

114   chemiluminescence), NO_y (chemiluminescence), peroxyacetyl nitrate (PAN; custom gas chromatograph), and

115   meteorological parameters (e.g., Weiss-Penzias et al., 2006; Briggs et al., 2016). Data reported in this study are

116   5-min averages. During this study, an HR-AMS (DeCarlo et al., 2006) was deployed downstream of a

117   thermodenuder (TD) to measure the size-resolved composition and volatility of NR-PM_1. These are the first real-

118   time aerosol chemical measurements at MBO. The TD consists of a heated tube followed by a heated adsorption

119   section that uses carbon cloth to prevent recondensation of organic vapors (Fierz et al., 2007). The TD was

120   automated using a custom program to step through 12 different temperatures ranging from 30 to 200°C, at 10 min

121   time intervals. Changes in mass and chemical composition of NR-PM_1 as a result of aerosol evaporation were

122   quantified by the HR-AMS by alternating sampling between the TD and the bypass (BP) ambient sampling mode

123   every 5 min. During BP mode, the temperature in the heated section ramped up to the next setting and reached

124   thermal stability before switching back to TD mode. The switching between sampling modes was triggered by a

125   digital output signal from the HR-AMS which was synchronized to the HR-AMS averaging intervals and was

126   achieved using an actuated 3-way ball valve. Aerosol residence time in the TD was 8.2 s at the experimental flow

127   rate (1.1 L min^{-1}). Particle losses within the TD mode (~ 5%) due to diffusional and thermophoretic forces were

128   quantified based on the behavior of ammonium sulfate.

129   **2.3   HR-AMS data analysis**

130   The HR-AMS was operated in the ion optical "V-mode" with reduced micro-channel plate bandwidth due to

131   signal interference at MBO, and was calibrated following standard protocols described in detail in Collier et al.

132   (2016). Data analyses were performed utilizing AMS analysis toolkit SQUIRREL v1.53 and PIKA v1.12 in Igor Pro

133   6.34A (Wavemetrics, Inc., Lake Oswego, OR). Default relative ionization efficiency (RIE) values were assumed for

134   organics (1.4), nitrate (1.1), and chloride (1.3), while an RIE value of 5 was determined for ammonium and 1.32 for

135   sulfate following the analysis of pure NH_4NO_3 and $(NH_4)_2SO_4$, respectively. A time- and composition-dependent

136   collection efficiency (CE) was applied based on the algorithm by Middlebrook et al. (2012), leading to an average

137   (±1σ) CE of 0.56 (±0.12). Time-dependent gas phase CO_2^+ subtraction was performed to improve the determination

138   of OA, which is critical for low OA concentration periods (Collier and Zhang, 2013). The mass concentrations of

139   ammonium, nitrate, chloride, and sulfate were determined from PIKA analysis of the high-resolution mass spectra

140   (HRMS) whereas organic concentrations came from SQUIRREL analysis of the unit mass resolution (UMR) data.

141   The detection limits of organics, sulfate, nitrate, ammonium, and chloride, defined as 3 times the standard deviations

142   (3σ) of the corresponding signals in particle-free ambient air, were 28.1, 4.5, 2.3, 9.6, and 3.0 ng m^{-3}, respectively,

Atmospheric
Chemistry
and Physics
Discussions

143   for an averaging time of 5 min. Atomic oxygen-to-carbon (O/C) and hydrogen-to-carbon (H/C) ratios and the

144   organic mass-to-carbon (OM/OC) ratio were determined using the Improved-Ambient (IA) method (Canagaratna et

145   al., 2015). We also reported the ratios determined using the previously published Aiken-Ambient (AA) method

146   (Aiken et al., 2008) in order to compare with literature results. As shown in Fig. S1 in the Supplement, the O/C, H/C,

147   and OM/OC values determined from the two methods correlate tightly (r^2 = 0.99), and the IA method reports 29%,

148   5%, and 31%, respectively, higher values compared to the AA method.

149   Positive Matrix Factorization (PMF) was executed using the PMF2 algorithm (Paatero and Tapper, 1994) in the

150   PET v2.05 program (Ulbrich et al., 2009). The spectral matrices of organic and inorganic species were combined

151   (Sun et al., 2012) and the ion signals were expressed in nitrate-equivalent concentrations. Periods with organic

152   concentration below 1.5 μg m^{-3} were excluded from PMF analysis due to low signal-to-noise (S/N) ratios, which

153   could prevent model convergence. The HRMS of organic ions at m/z 12 – 180 and the UMR signals at m/z 181 –

154   350 were included. For inorganics, only the major ions for each species were included, i.e., SO$^+$, SO$_2^+$, HSO$_2^+$, SO$_3^+$,

155   HSO$_3^+$, and H$_2$SO$_4^+$ for sulfate, NO$^+$ and NO$_2^+$ for nitrate, NH$^+$, NH$_2^+$, and NH$_3^+$ for ammonium, and HCl$^+$ for

156   chloride. Cl$^+$ was not included due to low S/N. Data preparation prior to PMF analysis followed the steps outlined in

157   the Table 1 of Zhang et al. (2011). After PMF analysis, the mass concentration of each OA factor was derived from

158   the sum of organic signals in the corresponding mass spectrum after applying proper CE and RIE. The solutions for

159   3 to 8 factors were explored with varying rotational parameters (-0.5 ≤ FPEAK ≤ 0.5, in increments of 0.1). After a

160   detailed evaluation of mass spectral profiles, temporal trends, diurnal variations, and correlations with external

161   tracers, the five-factor solution with FPEAK = 0 was chosen. The diagnostic information for five-factor solution is

162   shown in Fig. S2. In comparison, the four-factor solution resulted in large residual signals, indicating that an

163   additional factor was needed to explain the variation in the data, whereas the six-factor solution showed indications

164   of factor splitting, suggesting that too many factors were introduced (Fig. S3).

165   The concentrations of OA factors at different TD temperatures were determined via multivariate linear regression

166   of the HRMS of OA after TD against the HRMS of the 5 OA factors determined from PMF of the ambient OA data

167   following the procedures given in Zhou et al. (2016). The mass fraction remaining (MFR) of a factor at each TD

168   temperature was then determined as the slope from orthogonal fit between the time series after TD and the ambient

169   time series (Fig. S4). Thermograms, which describe the MFR as a function of temperature, have been corrected for

170   particle losses in the TD mode. Aerosol data reported here have all been converted to concentrations at standard

171   temperature and pressure (STP, 273 K, 1 atmosphere).

172   **2.4   Back trajectory analysis and calculations of plume transport time and cumulative solar radiation**

173   The HYbrid Single Particle Lagrangian Integrated Trajectory (HYSPLIT) model backward air mass trajectories

174   (Draxler, 1998) were initiated from MBO at one-hour intervals throughout the campaign period. Three-day

175   backward trajectories using the 40 km resolution US Eta Data Assimilation System (EDAS) meteorological data

176   (http://ready.arl.noaa.gov/HYSPLIT.php) were calculated at a starting height of 1500m above ground level.

177   Meteorological variables (e.g. solar radiation and relative humidity (RH)) along the trajectories were also output. By

178   overlapping the back trajectories with MODIS fire hotspots, we estimated the transport times for BB plumes that

179 unambiguously passed over active fire sources (Collier et al., 2016). In addition, we also estimated the cumulative

180 solar radiation exposure and average RH for these plumes during the period between emission at fire source and

181 arrival at MBO.

182 **3   Results and discussions**

183 **3.1   Observations of wildfire-influenced air masses at MBO**

184   Fig. 2 provides an overview of the meteorological conditions, trace gases mixing ratios, and aerosol

185 concentration and composition during the sampling period (July 25 – August 25, 2013). The summit air was cool

186 (average temperature of 11.2 ± 4 °C) and dry (average RH of $46 \pm 21\%$), although there were periods (e.g., August

187 16 and August 23) when MBO was in low clouds and measured RH reached 98%. Wind was generally strong

188 (average = 5.7 ± 3.4 m s^{-1}) with a dominant flow from the west and southwest direction, which provides suitable

189 conditions for long-range transport of fire smoke from Northern California and Southwest Oregon. Indeed, the

190 bivariate polar plots of total NR-PM$_1$, submicrometer aerosol light scattering at 550 nm (σ_{550nm}), and CO (Fig. 1b, 1d,

191 and 1e) calculated using the OpenAir software (Carslaw and Ropkins, 2012) all show the highest values at a wind

192 speed of ~ 13 m s^{-1} from the southwest direction, where the major complex fires were located (Fig. 1a).

193   The average NR-PM$_1$ concentration during the entire sampling period was 15.1 μg m^{-3} and 93% was contributed

194 by organics (Fig. 1c). However, aerosol concentrations and composition changed dynamically. Clean periods of low

195 concentrations of aerosol (NR-PM$_1$ < 10 μg/m^3) and gas-phase pollutants (e.g., CO, NO$_y$, and PAN) were observed

196 for the first week of sampling (July 25 – 30) and during August 18 – 21 (Fig. 2d – 2f). During these periods,

197 ammonium sulfate contributed up to 90% of the NR-PM$_1$ mass (Fig. 2g) and the OA spectra showed low

198 abundances of $C_2H_4O_2^+$ ($m/z = 60.021$) and $C_3H_5O_2^+$ ($m/z = 73.029$), which are ion fragments of anhydrous sugar

199 (e.g., levoglucosan) and HR-AMS tracers for BB (Alfarra et al., 2007). The fraction of the signal at $m/z = 60$ (mostly

200 $C_2H_4O_2^+$) in OA spectrum (f$_{60}$) was generally below 0.3% (Fig. 2h), indicating minimal BB influence during "clean"

201 periods (Cubison et al., 2011).

202   In contrast, the other periods were characterized by higher f$_{60}$ (up to 2%), elevated NR-PM$_1$ concentration (up to

203 ~ 210 μg m^{-3}), and larger OA fraction (generally > 90% of NR-PM$_1$; Fig. 2e – 2g). In addition, σ_{550nm} (up to ~ 670

204 Mm^{-1}), CO (up to ~ 700 ppbv), NO$_y$ (up to ~ 6.5 ppbv), and PAN (up to ~ 2.2 ppbv) all increased dramatically

205 during high f$_{60}$ periods (Fig. 2d – 2e). In fact, the time series of all these parameters correlate tightly, with Pearson's

206 r^2 in the range of 0.66 – 0.94 (Fig. S5). These observations highlight the frequent and significant impacts of wildfire

207 emissions on air quality and atmospheric chemistry in the Pacific Northwest region. Note that although potassium

208 (K) is frequently used as a tracer for BB aerosol, K concentration was very low throughout this study, indicating low

209 K contents in wildfire emissions in the western US. Similarly, Maudlin et al. (2015) observed no strong

210 enhancement of K in wildfire smokes originated from California and Oregon and concluded that it is not a reliable

211 tracer for BB in this region.

212 **3.2   Impacts of wildfires on regional aerosol characteristics**

Atmospheric
Chemistry
and Physics
Discussions

3.2.1. Changes of aerosol concentration and composition due to wildfires

Given that f_{60} is a marker for the influence of BB emissions on OA composition, we divided the entire campaign into three regimes based on the f_{60} value: (1) "No BB" for periods with negligible BB influence and $f_{60} \leq 0.3\%$; (2) "BB Infl" for periods with detectable BB influences and moderately elevated f_{60} values (0.3% - 0.5%); and (3) "BB Plm" for periods with $f_{60} > 0.5\%$, indicating intense and less processed BB events. Note that periods with very low OA concentrations (< 1 µg/m^3), e.g., August 18 – 21, were classified as "No BB" regardless of the nominal f_{60} values. The average ($\pm 1\sigma$) f_{60} values were 0.18 ± 0.10%, 0.43 ± 0.05% and 0.77 ± 0.29% for "No BB", "BB Inf", and "BB Plm" periods, respectively (Fig. 3 and Table S1). Similarly, the average mixing ratios of CO, a gaseous pollutant released from combustion, increased from 87.8 ± 17.9 ppbv during "No BB" to 121.4 ± 24.8 ppbv during "BB Infl" and 178.3 ± 68.8 ppbv during "BB Plm" periods.

Fig. 3 shows the comparisons of gas and particle phase properties among the three regimes to illustrate the strong effects that wildfires have on gases and aerosol composition in the Pacific Northwest region. For example, the average NR-PM$_1$ concentration was only 3.7 (± 4.2) µg m^{-3} during "No BB" but increased by ~ 4 and ~ 7 times, respectively, during "BB Infl" (13.4 ± 7.1 µg m^{-3}) and "BB Plm" (25.7 ± 19.9 µg/m^3) periods. Aerosol measured at MBO during "BB Plm" periods was predominantly organic (94.6% of NR-PM$_1$ mass; Fig. S6c). The fraction of OA in BB aerosols may be fuel dependent, for instance, high values have been reported for ponderosa pine smoke emissions (99%) (Lewis et al., 2009) and somewhat lower values have been reported for forest fires in south-western Amazon (93%) (Artaxo et al., 2013) and North America boreal forests (87%) (Kondo et al., 2011), and agricultural fires in west Africa (85%) (Capes et al., 2008). Even lower values were observed in eastern Mediterranean wildfires (51.4%) (Bougiatioti et al., 2014) and Asian fires (60%) (Kondo et al., 2011). Since temperate evergreen vegetation was likely the dominant fuel during this campaign, the high OA/PM$_1$ ratio observed in this study appears consistent with those of ponderosa pine.

In addition to OA, concentrations of nitrate, ammonium, and chloride all showed substantial increases that correlated with wildfire impacts (Fig. 3 and Table S1). Nitrate, in particular, displayed large temporal variations that correlated with wildfire plume influences and its concentration in the "BB Plm" regime was on average ~ 11 times greater than the "No BB" regime. Nitrate appeared to be bulk neutralized based on comparing the total molar equivalent of inorganic anions (i.e., sulfate, nitrate and chloride) to that of ammonium (Zhang et al., 2005) during wildfire-influenced periods (Fig. S7a) and the signal ratios of NO^+ to NO_2^+ observed in particles during these periods (2.15 ± 0.006) were very similar to the ratio measured for pure NH_4NO_3 particles (2.2; Fig. S7b), indicating that nitrate was mostly in the form of NH_4NO_3. Sulfate, on the other hand, displayed milder temporal variation with poor correlation with BB tracers (Fig. 2d-f), indicating that forest fires in this region are not a significant source of sulfate aerosol. Collier et al. (2016) came to a similar conclusion through examination of aerosol enhancement ratios in transported BB plumes.

Significant enhancements due to wildfires emissions were also observed for PAN and NO_y (Fig. 3). However, the mixing ratios of NO_x (mostly as NO_2) were comparable among the three regimes. As a result, the fractional contributions of PAN and particulate nitrate to total NO_y both increased due to wildfire influence (Fig. S8). Considering that MBO was hours downwind of wildfire sources during this study, this observation is consistent with

Atmospheric
Chemistry
and Physics
Discussions

250   the findings of Akagi et al. (2012) that NO_x emitted from BB is rapidly converted to PAN and particulate nitrate

251   during plume transport, which reflects high levels of acetaldehyde in fire plumes (Akagi et al 2011). The influence

252   of wildfire emissions on O_3 at MBO appears to be complex (Fig. 2c). The average O_3 mixing ratio in both "BB Infl"

253   (49.1 ppbv) and "BB Plm" (47.3 ppbv) regimes were higher than during the "No BB" (44.7 ppbv) periods (Fig. 3).

254   Similar observations were made previously, which indicate that O_3 tends to peak downwind of fire sources as a

255   result of the interplay of fire emissions (precursors and reactants) and chemical reactions (Jaffe and Wigder, 2012;

256   Wigder et al., 2013; Briggs et al., 2016).

3.2.2. Influence of wildfires on organic aerosol chemical properties

258   In order to demonstrate the influence of wildfires on bulk OA chemistry at MBO, the average HRMS of OA for

259   each of the three regimes are shown in Fig. S6. OA was generally highly oxidized under all three regimes and the

260   O/C of OA generally decreased as BB influence increased. In addition, ions larger than 100 amu ($f_{m/z>100}$)

261   contributed a larger fraction of the total organic signal during "BB Plm" periods (11%) compared to "No BB"

262   periods (5%), consistent with BBOA containing a larger fraction of high molecular weight compounds (Ge et al.,

263   2012a; Lee et al., 2016). OA in "No BB" air masses had an average O/C of 0.84 (O/C$_{AA}$, i.e., O/C calculated with

264   Aiken-Ambient method, is 0.63) and H/C of 1.48 (H/C$_{AA}$ = 1.29), in agreement with previous HR-AMS

265   measurements of free tropospheric OA at mountaintop sites (e.g., Sun et al., 2009; Rinaldi et al., 2015). The average

266   O/C for "BB Infl" and "BB Plm" periods were 0.77 (O/C$_{AA}$ = 0.60) and 0.69 (O/C$_{AA}$ = 0.53), respectively,

267   substantially higher than previously reported O/C for fresh BB emissions. For example, laboratory experiments

268   reported O/C$_{AA}$ in the range of 0.15 – 0.60 for POA from BB, depending on fuel type, burning condition, and burn

269   mass (Heringa et al., 2011; Ortega et al., 2013). The high O/C observed for BB-influenced OA at MBO indicates

270   that they were likely a combination of primary and secondary components with the secondary portion having a

271   substantial contribution to the bulk OA.

3.3   Aerosol source apportionment and contributions of primary and secondary BBOA at MBO

273   In order to gain further insight into the influences of different sources and processes on OA concentration and

274   composition at MBO, we performed PMF analysis on the HRMS of all NR-PM$_1$ species acquired during this study.

275   PMF is commonly applied to the organic mass spectral matrix to determine distinct OA factors (Zhang et al., 2011

276   and references therein), but conducting PMF analysis on the combined spectra of organic and inorganic aerosols

277   allows for deriving additional information, e.g., the distributions of inorganic signals among different factors and the

278   nominal acidity of the factors, which benefits the interpretation of the sources, chemical characteristics, and

279   evolution processes of OA (Sun et al., 2012). For this study, a total of five OA factors were identified, including

280   three different BB-related aerosol types, i.e., BBOA-1 (O/C = 0.35), BBOA-2 (O/C = 0.60), and BBOA-3 (O/C =

281   1.06), and two distinct OOA factors, i.e., a less oxidized OOA associated with boundary layer (BL) dynamics (BL-

282   OOA, O/C = 0.69) and a more oxidized low-volatility OOA representing free-troposphere aerosol (LV-OOA, O/C =

283   1.09). Unlike the two OOAs, the three distinct BBOA factors all showed high correlations with CO (r^2 = 0.70 - 0.86;

284   Table S2) and displayed sporadic, high amplitude events with large enhancements in concentrations during wildfire-

Atmospheric
Chemistry
and Physics
Discussions

285   influenced periods (Fig. 4a-c). In addition, the polar plots of all the BBOAs showed clear concentration hotspots in

286   the southwest direction at high wind speed (Fig. 5a-c), indicative of their associations with wildfire plumes

287   originating from SW Oregon and NW California (Fig. 1). Nevertheless, the three BBOAs are distinctly different in

288   terms of mass spectral profiles (Fig. 4k-m and Fig. S9), oxidation degrees, and volatility (Fig. 5g), likely due to

289   different extents of aging and/or processing pathways.

290   Among the three BBOA factors, BBOA-1 had the lowest O/C (0.35) and the highest H/C (1.76) and f_{60} (2.2%)

291   (Fig. 4k). In addition, the mass spectrum of BBOA-1 showed prominent signals of $C_2H_3^+$, CHO^+, $C_4H_7^+$, $C_4H_9^+$, and

292    $C_9H_7^+$, markers for chemically-reduced aerosols, and a high abundance of ions larger than 100 amu ($f_{m/z>100}$ = 25%;

293   Fig. 4k and 4k'). The UMR spectrum of BBOA-1 at m/z > 180 exhibited a "picket fence" fragmentation pattern

294   where groups of peaks have 14 amu separation, suggesting the occurrence of molecules with hydrocarbon moieties

295   containing different units of the CH_2 group. The time series of BBOA-1 correlated tightly with those of $C_2H_4O_2^+$ and

296    $C_4H_9^+$ (r^2 = 0.94 and 0.95, respectively; Table S2), tracers for primary emissions. Furthermore, BBOA-1 appeared to

297   have a strong point source SW of MBO and peaked in association with high wind speeds suggesting that it could be

298   associated with plumes experiencing shorter transport times relative to plumes from equidistant fire sources (Fig.

299   5a). Together, these observations suggest that BBOA-1 was primarily associated with fresher and less processed air

300   masses from BB sources. In addition, BBOA-1 was found to be semivolatile (Fig. 5g), which is consistent with

301   previous findings that a majority (50% - 80%) of the POA in BB emissions is semivolatile (May et al., 2013). The

302   semivolatile behavior of BBOA-1 also explains the high degree of correlation between BBOA-1 and nitrate (r^2 =

303   0.60; Fig. 4a and Table S2), a secondary species that is often found to correlate with semivolatile OOA (SV-OOA)

304   (Zhang et al., 2011). However, despite being a secondary component, nitrate displayed tight correlations with

305   primary smoke markers, i.e., $C_2H_4O_2^+$ and $C_3H_5O_2^+$, at MBO (Fig. S10). Therefore, it appears that fast processing

306   near the fire sources led to the rapid conversion of NO_x to more oxidized compounds such as PAN and nitrate.

307   Based on these results, we infer that BBOA-1 represents fresher BB emissions and might be a surrogate for primary

308   BBOA. On average, BBOA-1 comprised 20% of total OA mass during this study (Fig. 5f), suggesting that fresh BB

309   emissions exerted a significant impact on regional air masses.

310   The more oxygenated BBOA-2 (O/C = 0.60; H/C = 1.72) accounted for an average 17% of the total OA mass

311   (Fig. 5f). Its mass spectrum displayed characteristics of aged BBOA with lower abundances of $C_2H_4O_2^+$ (f_{60} =

312   1.1%), $C_xH_y^+$ ions (31%), and ions > 100 amu ($f_{m/z>100}$ = 17%) compared to BBOA-1 (Figs. 4l, 4l' and S9b).

313   BBOA-2 also showed a somewhat less volatile profile compared to BBOA-1, especially at TD temperature < 150°C

314   (Fig. 5g). In addition, the temporal trend of BBOA-2 displayed tight correlations with tracers for carboxylic acids,

315   e.g., CHO_2^+ and CO_2^+ (r^2 of 0.91 and 0.79, respectively; Fig. 4b and Table S2) but lower correlations with nitrate,

316    $C_2H_4O_2^+$, and $C_4H_9^+$. These results suggest that BBOA-2 was more chemically processed and likely contained

317   secondary products. Indeed, the polar plot of BBOA-2 (Fig. 5b) displayed a more dispersed pattern of sources

318   compared to BBOA-1 with hotspots located in various directions. Nevertheless, the occurrence of a high

319   concentration band at 5 - 15 m s^{-1} in the SW direction suggests important BBOA-2 sources from similar distances

320   and locations as BBOA-1. The dispersed source features are further evidence that BBOA-2 is more secondary in

321   nature compared to BBOA-1 and is likely more aged.

322   BBOA-3 contrasts strongly with BBOA-1 and BBOA-2 in chemical composition. The HRMS of BBOA-3 had a

323   very low $C_2H_4O_2^+$ signal ($f_{60} = 4 \times 10^{-8}$), a relatively high intensity of CO_2^+ ($f_{44} = 0.215$) and a high degree of

324   oxidation (O/C = 1.07; Fig. 4m), all of which highly resemble those of LV-OOA (Fig. 4o). However, the mass

325   spectra at large m/z's indicated distinct chemical differences between BBOA-3 and LV-OOA (Fig. 4m' and 4o'), as

326   there appeared to be a higher abundance of high molecular weight species in BBOA-3. In addition, the temporal

327   variation patterns of BBOA-3 and LV-OOA were dramatically different ($r^2 = 0.07$) and BBOA-3 closely correlated

328   with CO ($r^2 = 0.86$; Fig. 4c and Table S2) whereas LV-OOA did not ($r^2 = 0.008$). As shown in Fig. 5, the polar plot

329   of BBOA-3 showed a high concentration band from SW at a wind speed of 5 – 15 m s^{-1}, which overlaps with the hot

330   spot shown in the BBOA-1 polar plot (Fig. 5a). These results suggest that BBOA-3 was likely formed both through

331   rapid processing near the wildfire source and during transport to MBO.

332   Another important characteristic of BBOA-3 is that it appeared to be composed of some very low-volatility

333   compounds. As shown in Fig. 5g, ~ 60% of its mass remained in the aerosol phase at a temperature of 200 °C. This

334   observation is consistent with previous studies which have observed the presence of low-volatility and extremely

335   low volatility BBOA materials in aged wildfire plumes (Lee et al., 2016; Paciga et al., 2016) and in SOA produced

336   from major organic gases from BB (e.g., phenols) (Yu et al., 2016). It is important to note that the highly oxidized

337   BBOA-3 on average accounted for 31% of the total OA mass during this study, which implies that a significant

338   fraction of the highly aged BBOA may appear indistinguishable from OOA from other sources due to mass spectral

339   similarities (e.g., low f_{60} and high f_{44}) and hence would lead to an underestimation of the influence of BB emissions

340   on a regional scale.

341   BL-OOA and LV-OOA accounted for the remaining 32% of total OA mass during this study. These two OOAs

342   were not associated with BB, as indicated by low f_{60} (Fig. 4n and 4o) and a lack of correlation with BB tracers

343   (Table S2). BL-OOA was relatively oxidized (O/C = 0.69; Fig. 4n) and appeared significantly less volatile than

344   nitrate but more volatile than sulfate (Fig. 5g). BL-OOA showed a distinct diurnal cycle highly resembling that of

345   water vapor (Fig. 5i), which is a tracer for BL upslope flow during the daytime at MBO (Weiss-Penzias et al., 2006).

346   Photochemical production of OA in the early afternoon may also contribute to the daytime increase of BL-OOA.

347   Furthermore, the time series of BL-OOA correlated with $CH_3SO_2^+$ (Fig. 4d and Table S2), a signature ion for

348   methanesulfonic acid (MSA) (Ge et al., 2012b). MSA is typically associated with marine sources but has been found

349   to have terrestrial sources as well (Ge et al., 2012b; Young et al., 2016). All these results suggest the influence of BL

350   dynamics on BL-OOA. In comparison, the LV-OOA was highly oxidized (O/C = 1.09) with a pronounced CO_2^+

351   peak in the spectrum (Fig. 4o). In addition, Fig. 5g indicates that LV-OOA shared a similar volatility profile as

352   sulfate, showing no sign of evaporation until the TD temperature reached nearly 130°C, consistent with LV-OOA

353   previously determined in other ambient studies (Huffman et al., 2009; Paciga et al., 2016). The diurnal pattern of

354   LV-OOA appeared to be rather flat (Fig. 4j) and its polar plot had the most dispersed feature among all factors (Fig.

355   5e). All these observations suggest that this factor is representative of free tropospheric aerosol.

356   **3.4   A case study of the aging of BBOA in wildfire plumes**

Atmospheric
Chemistry
and Physics
Discussions

357   Based on MODIS fire hotspot information, the Salmon River Complex fire (SRCF) was continuously burning

358   from August 13 to August 17 (Fig. 6a). Three-day HYSPLIT back trajectories suggest that air masses arriving at

359   MBO from August 14 22:00 to August 16 09:00 passed over the SRCF (Fig. 6a), consistent with the observations of

360   persistent SW wind at MBO during this time period (Fig. 6c). MODIS also detected a few hotspots from the

361   Whiskey Complex Fire (~ 43°N, 122.8°W) intermittently on August 15 but the fire was much weaker compared to

362   SRCF as indicated by the lower fire radiative power (FRP, Fig. 6a). We therefore assume that the emissions arriving

363   at MBO during this time period were from a single source and therefore consistent in transport distance and fuel

364   type. Combining MODIS fire hotspots and back-trajectories, we estimated that the transport time of SRCF plumes

365   ranged from 8 to 11 hours before being sampled at MBO.

366   In order to examine how atmospheric aging affects BBOA chemistry, we calculated cumulative solar radiation

367   ($\sum$SR) and average RH over the total transport time (from source to MBO) for each trajectory and plotted them

368   versus air mass arrival time in Fig. 6b. $\sum$SR denotes the total amount of solar radiation that the smoke plumes were

369   exposed to during transport and can be used as an indicator for the extent of photochemical aging assuming the

370   plumes were optically thin. RH in the air mass history was relatively stable, however $\sum$SR clearly varied throughout

371   the measurement period such that some BB plumes experienced more solar radiation than others and some were

372   transported exclusively at night. Furthermore, the burn conditions were modestly constant during this period with an

373   average modified combustion efficiency (MCE) value of 0.88 ($\pm$ 0.03) for the BB plumes that met the criteria for

374   MCE calculation (Collier et al., 2016). Furthermore, the MCE values showed no differences between nighttime and

375   daytime plumes and didn't correlate with $\sum$SR (Fig. S11). These conditions, together with the high emissions

376   concentrations for both gas and particle phase components (Fig. 6d-f), provide a near ideal case study where

377   atmospheric aging is likely the largest factor affecting the chemical evolution of BBOA.

378   During this SRCF case study period, CO, NO_y, and PAN mixing ratios observed at MBO exhibited similar trends

379   that varied dynamically and correlated well with the fresh BBOA-1 factor (Fig. 6d - f). In addition, OA was

380   overwhelming dominated by BBOAs, which summed to contribute 80% - 99% of total OA mass (Fig. 6g). The

381   chemical parameters of OA and the fractional contributions of each BBOA factor appear to be related to $\sum$SR (Figs.

382   6g and 6h). In order to investigate the chemical evolution of BBOA, we reconstructed the time series and the

383   chemistry parameters of total BBOA (= BBOA-1 + BBOA-2 + BBOA-3) from the residual matrix of organic

384   aerosol after subtracting the contributions from BL-OOA and LV-OOA. The carbon oxidation state ($OS_c = 2 \times O/C$

385   – H/C; (Kroll et al., 2011)) of total BBOA showed a clear increasing trend with respect to $\sum$SR, consistent with the

386   trends of O/C and f_{44}, while H/C, f_{60}, and $f_{m/z>100}$ of total BBOA showed decreasing trends with $\sum$SR (Fig. 7). These

387   results suggest oxidation of anhydrous sugar and other BBOA components due to photochemical aging, consistent

388   with previous observations in the laboratory (Grieshop et al., 2009; Hennigan et al., 2011; Ortega et al., 2013) and

389   field (Cubison et al., 2011; May et al., 2015). In addition, the negative correlation between BBOA-1 and $\sum$SR and

390   the positive correlations of BBOA-2 and BBOA-3 with $\sum$SR (Fig. 7) corroborated our earlier assumption that

391   BBOA-2 and BBOA-3 represented more aged, secondary BBOA whereas BBOA-1 represented primary BBOA.

392   We classify the plumes according to $\sum$SR and designate those as night-time transported if $\sum$SR was below 500 W

393   m^{-2}, and the rest as day-time transported. OA concentration and CO mixing ratio were tightly correlated, with $r^2 =$

Atmospheric
Chemistry
and Physics
Discussions

394   0.88 and 0.94 for night- and day-time transported plumes, respectively (Fig. 8a). CO has been commonly used as a

395   stable plume tracer to account for dilution and the slope obtained from orthogonal fitting between OA and CO is

396   defined as the enhancement ratio (i.e., $\Delta OA/\Delta CO$). Change of $\Delta OA/\Delta CO$ during plume transport indicates the

397   influence of factors other than dilution, e.g., SOA formation or OA evaporation. For the SRCF case study,

398    $\Delta OA/\Delta CO$ was very similar for the day-plumes and the night-plumes: 0.28 ± 0.014 vs. 0.27 ± 0.005 µg m^{-3} ppbv^{-1}

399   respectively (Fig. 8a), suggesting no net OA mass enhancement due to photochemical aging. This is consistent with

400   the findings of Collier et al. (2016), which compared selected BB events from this dataset measured at MBO to

401   those aboard a research aircraft sampling fresher plume emissions and found very similar OA enhancements

402   between the fresher and more aged emissions. However, compared to daytime-plumes, OA for plumes transported

403   during night time was less oxidized (Fig. 8c and 8d) and was dominated by the fresh BBOA-1 (53%), followed by

404   the most oxidized BBOA-3 (24%), and intermediately oxidized BBOA-2 (15%; Fig. 8b). By contrast, daytime

405   plumes were characterized by a significant decrease in the mass fraction of BBOA-1 (37%) coupled with increases

406   in the BBOA-2 (20%) and BBOA-3 (37%). This is corroborated by the significant differences in chemical

407   composition for the two types of plumes, where the average HRMS (Fig. 8c and 8d) indicated that the BBOA in

408   day-time plumes had a higher degree of oxidation (average O/C = 0.66) compared to the night plumes (O/C = 0.55).

409   These observations together suggest that although net OA production was conserved with higher photochemical

410   aging, BBOA was chemically transformed, likely due to oxidative processing in both gas and particles phases

411   followed by fragmentation and volatilization.

4   Summary and conclusions

413   We have characterized the chemical composition and properties of aerosols at a high elevation site that was

414   heavily impacted by wildfire smoke plumes in the western US during the BBOP campaign in summer 2013. The

415   sampling site was located on the summit of Mt. Bachelor, an isolated volcanic peak, in central Oregon. It was

416   impacted by regional wildfire emission during a majority of the campaign and saw intense BB plumes with elevated

417   air pollutants (up to 700 ppbv of CO and ~ 210 µg m^{-3} of NR-PM$_1$). The average ($\pm 1\sigma$) NR-PM$_1$ mass concentration

418   was 22.4 (± 17.7) µg m^{-3} during fire-impacted periods, mostly due to OA that dominated the NR-PM$_1$ composition.

419   In contrast, the average NR-PM$_1$ concentration was only 3.7 µg m^{-3} over periods free of BB influence and the

420   aerosols contained a high mass fraction of ammonium sulfate (up to ~ 90%). In addition to increasing regional

421   aerosol concentrations, wildfires in the Pacific Northwest region also significantly increased the mixing ratios of CO,

422   NO$_y$, and PAN, although NO$_x$ and O$_3$ displayed more complex behavior.

423   PMF analysis identified three types of BBOA that together accounted for 68% of the OA mass during this study,

424   in addition to two types of OOA representing regional air conditions. The time series of all BBOA factors displayed

425   dynamic variations that tightly correlated with those of CO and aerosol light scattering. Yet the three BBOAs were

426   significantly different both chemically and physically and appeared to have been subjected to different degrees of

427   atmospheric processing. BBOA-1 appeared to represent fresh wildfire emissions and featured semivolatile behavior,

428   low O/C, a larger fraction of anhydrous sugar (f$_{60}$ = 2.2%), and a strong association with active wildfire sources. On

429   the other hand, BBOA-2 and BBOA-3 represented more aged BB emissions and showed higher oxidation degree,

Atmospheric
Chemistry
and Physics
Discussions

430 lower f_{60}, significantly lower volatilities, and more dispersed source regions. BBOA-3, in particular, had an O/C of

431 1.06, very low volatility, and almost no contribution from f_{60}, and thus appeared to be chemically similar to highly

432 oxidized SOA observed in the atmosphere. Nevertheless, BBOA-3 is substantially different than the LV-OOA factor

433 identified in this study; in addition to dramatically different temporal variation patterns, BBOA-3 also seemed to be

434 composed of a higher fraction of high molecular weight species as well as compounds of extremely low volatilities.

435 A case study using consecutive BB plumes transported from the same fire source was performed to examine in

436 detail the environmental factors leading to BBOA evolution. The BB plumes were associated with fires of similar

437 modified combustion efficiencies but were exposed to a wide range of photochemical aging, as indicated by the

438 cumulative solar radiation along the trajectory history from fire source to the sampling site. The results showed that

439 photochemical aging led to more oxidized OA with higher mass fractions of aged BBOA (i.e., BBOA-2 and BBOA-

440 3) and a lower fraction of fresh BBOA-1. Although BBOA in daytime plumes were chemically more processed than

441 nighttime plumes, the enhancement ratios of OA relative to CO were very similar under the night-time and day-time

442 conditions (ΔOA/ΔCO = 0.28 ± 0.014 and 0.27 ± 0.005 µg m^{-3} ppbv^{-1}, respectively). One explanation for this

443 apparent lack of net SOA production in transported BB plumes is that SOA formation in BB emissions was balanced

444 by POA loss, likely due to oxidation followed by fragmentation and volatilization.

445 Over the entire period of this study, the aged BBOA-2 and BBOA-3, most of which were likely secondary, on

446 average made up ~ 50% of the OA mass observed at MBO. Aged BBOAs were present at significant concentrations

447 even in relatively fresh plumes (~ 6-12 hr of atmospheric aging). These results suggest that BB emissions undergo

448 substantial chemical processing which commences directly after emission and continues during atmospheric

449 transport, forming and transforming aerosols that can significantly influence air quality and atmospheric chemical

450 composition at downwind sites with important implications for health and climate.

451 **Acknowledgements**

461 **References**

462 Abel, S. J., Haywood, J. M., Highwood, E. J., Li, J., and Buseck, P. R.: Evolution of biomass burning aerosol properties from an

463 agricultural fire in southern Africa, Geophysical Research Letters, 30, 2003.

Atmospheric
Chemistry
and Physics
Discussions

464   Aiken, A. C., Decarlo, P. F., Kroll, J. H., Worsnop, D. R., Huffman, J. A., Docherty, K. S., Ulbrich, I. M., Mohr, C., Kimmel, J.
465   R., Sueper, D., Sun, Y., Zhang, Q., Trimborn, A., Northway, M., Ziemann, P. J., Canagaratna, M. R., Onasch, T. B., Alfarra, M.
466   R., Prevot, A. S. H., Dommen, J., Duplissy, J., Metzger, A., Baltensperger, U., and Jimenez, J. L.: O/C and OM/OC ratios of
467   primary, secondary, and ambient organic aerosols with high-resolution time-of-flight aerosol mass spectrometry, Environmental
468   Science & Technology, 42, 4478-4485, 2008.

469   Akagi, S. K., Yokelson, R. J., Wiedinmyer, C., Alvarado, M. J., Reid, J. S., Karl, T., Crounse, J. D., and Wennberg, P. O.:
470   Emission factors for open and domestic biomass burning for use in atmospheric models, Atmos. Chem. Phys., 11, 4039-4072,
471   2011.

472   Akagi, S. K., Craven, J. S., Taylor, J. W., McMeeking, G. R., Yokelson, R. J., Burling, I. R., Urbanski, S. P., Wold, C. E.,
473   Seinfeld, J. H., Coe, H., Alvarado, M. J., and Weise, D. R.: Evolution of trace gases and particles emitted by a chaparral fire in
474   California, Atmos. Chem. Phys., 12, 1397-1421, 2012.

475   Alfarra, M. R., Prevot, A. S. H., Szidat, S., Sandradewi, J., Weimer, S., Lanz, V. A., Schreiber, D., Mohr, M., and Baltensperger,
476   U.: Identification of the Mass Spectral Signature of Organic Aerosols from Wood Burning Emissions, Environmental Science &
477   Technology, 41, 5770-5777, 2007.

478   Artaxo, P., Rizzo, L. V., Brito, J. F., Barbosa, H. M. J., Arana, A., Sena, E. T., Cirino, G. G., Bastos, W., Martin, S. T., and
479   Andreae, M. O.: Atmospheric aerosols in Amazonia and land use change: from natural biogenic to biomass burning conditions,
480   Faraday Discuss., 165, 203-235, 2013.

481   Bond, T. C., Streets, D. G., Yarber, K. F., Nelson, S. M., Woo, J.-H., and Klimont, Z.: A technology-based global inventory of
482   black and organic carbon emissions from combustion, Journal of Geophysical Research: Atmospheres, 109, D14203, 2004.

483   Bougiatioti, A., Stavroulas, I., Kostenidou, E., Zarmpas, P., Theodosi, C., Kouvarakis, G., Canonaco, F., Prévôt, A. S. H., Nenes,
484   A., Pandis, S. N., and Mihalopoulos, N.: Processing of biomass-burning aerosol in the eastern Mediterranean during summertime,
485   Atmos. Chem. Phys., 14, 4793-4807, 2014.

486   Briggs, N. L., Jaffe, D. A., Gao, H., Hee, J., Baylon, P., Zhang, Q., Zhou, S., Collier, S., Sampson, P. D., and Cary, R. A.:
487   Particulate matter, ozone, and nitrogen species in aged wildfire plumes observed at the Mount Bachelor Observatory, Aerosol Air
488   Qual. Res., doi: 10.4209/aaqr.2016.03.0120, 2016. 2016.

489   Brito, J., Rizzo, L. V., Morgan, W. T., Coe, H., Johnson, B., Haywood, J., Longo, K., Freitas, S., Andreae, M. O., and Artaxo, P.:
490   Ground-based aerosol characterization during the South American Biomass Burning Analysis (SAMBBA) field experiment,
491   Atmos. Chem. Phys., 14, 12069-12083, 2014.

492   Canagaratna, M. R., Jimenez, J. L., Kroll, J. H., Chen, Q., Kessler, S. H., Massoli, P., Hildebrandt Ruiz, L., Fortner, E., Williams,
493   L. R., Wilson, K. R., Surratt, J. D., Donahue, N. M., Jayne, J. T., and Worsnop, D. R.: Elemental ratio measurements of organic
494   compounds using aerosol mass spectrometry: characterization, improved calibration, and implications, Atmos. Chem. Phys., 15,
495   253-272, 2015.

Atmospheric
Chemistry
and Physics
Discussions

496 Capes, G., Johnson, B., McFiggans, G., Williams, P. I., Haywood, J., and Coe, H.: Aging of biomass burning aerosols over West
497 Africa: Aircraft measurements of chemical composition, microphysical properties, and emission ratios, Journal of Geophysical
498 Research-Atmospheres, 113, 13, 2008.

499 Carslaw, D. C. and Ropkins, K.: openair - An R package for air quality data analysis, Environmental Modelling & Software, 27-
500 28, 52-61, 2012.

501 Collier, S. and Zhang, Q.: Gas-Phase CO_2 Subtraction for Improved Measurements of the Organic Aerosol Mass Concentration
502 and Oxidation Degree by an Aerosol Mass Spectrometer, Environmental Science & Technology, 47, 14324-14331, 2013.

503 Collier, S., Zhou, S., Onasch, T. B., Jaffe, D. A., Kleinman, L., Sedlacek, A. J., Briggs, N. L., Hee, J., Fortner, E., Shilling, J. E.,
504 Worsnop, D., Yokelson, R. J., Parworth, C., Ge, X., Xu, J., Butterfield, Z., Chand, D., Dubey, M. K., Pekour, M. S., Springston,
505 S., and Zhang, Q.: Regional Influence of Aerosol Emissions from Wildfires Driven by Combustion Efficiency: Insights from the
506 BBOP Campaign, Environmental Science & Technology, 50, 8613-8622, 2016.

507 Cubison, M. J., Ortega, A. M., Hayes, P. L., Farmer, D. K., Day, D., Lechner, M. J., Brune, W. H., Apel, E., Diskin, G. S., Fisher,
508 J. A., Fuelberg, H. E., Hecobian, A., Knapp, D. J., Mikoviny, T., Riemer, D., Sachse, G. W., Sessions, W., Weber, R. J.,
509 Weinheimer, A. J., Wisthaler, A., and Jimenez, J. L.: Effects of aging on organic aerosol from open biomass burning smoke in
510 aircraft and laboratory studies, Atmospheric Chemistry and Physics, 11, 12049-12064, 2011.

511 De Gouw, J. and Jimenez, J. L.: Organic Aerosols in the Earth's Atmosphere, Environmental Science & Technology, 43, 7614-
512 7618, 2009.

513 de Gouw, J. A., Warneke, C., Stohl, A., Wollny, A. G., Brock, C. A., Cooper, O. R., Holloway, J. S., Trainer, M., Fehsenfeld, F.
514 C., Atlas, E. L., Donnelly, S. G., Stroud, V., and Lueb, A.: Volatile organic compounds composition of merged and aged forest
515 fire plumes from Alaska and western Canada, Journal of Geophysical Research: Atmospheres, 111, D10303, 2006.

516 DeCarlo, P. F., Kimmel, J. R., Trimborn, A., Northway, M. J., Jayne, J. T., Aiken, A. C., Gonin, M., Fuhrer, K., Horvath, T.,
517 Docherty, K. S., Worsnop, D. R., and Jimenez, J. L.: Field-deployable, high-resolution, time-of-flight aerosol mass spectrometer,
518 Analytical Chemistry, 78, 8281-8289, 2006.

519 DeCarlo, P. F., Ulbrich, I. M., Crounse, J., de Foy, B., Dunlea, E. J., Aiken, A. C., Knapp, D., Weinheimer, A. J., Campos, T.,
520 Wennberg, P. O., and Jimenez, J. L.: Investigation of the sources and processing of organic aerosol over the Central Mexican
521 Plateau from aircraft measurements during MILAGRO, Atmos. Chem. Phys., 10, 5257-5280, 2010.

522 Dennison, P. E., Brewer, S. C., Arnold, J. D., and Moritz, M. A.: Large wildfire trends in the western United States, 1984–2011,
523 Geophysical Research Letters, 41, 2014GL059576, 2014.

524 Draxler, R. R., Hess, G. D. : An overview of the Hysplit-4 modeling system for trajectories, dispersion, and deposition, Aust.
525 Meteorol. Magn. , 47, 295-308, 1998.

526 Engelhart, G. J., Hennigan, C. J., Miracolo, M. A., Robinson, A. L., and Pandis, S. N.: Cloud condensation nuclei activity of
527 fresh primary and aged biomass burning aerosol, Atmos. Chem. Phys., 12, 7285-7293, 2012.

Atmospheric Chemistry and Physics

Discussions

Open Access

EGU

528 Engling, G., Herckes, P., Kreidenweis, S. M., Malm, W. C., and Collett Jr, J. L.: Composition of the fine organic aerosol in
529 Yosemite National Park during the 2002 Yosemite Aerosol Characterization Study, Atmospheric Environment, 40, 2959-2972,
530 2006.

531 Fierz, M., Vernooij, M. G. C., and Burtscher, H.: An improved low-flow thermodenuder, Journal of Aerosol Science, 38, 1163-
532 1168, 2007.

533 Ge, X. L., Setyan, A., Sun, Y. L., and Zhang, Q.: Primary and secondary organic aerosols in Fresno, California during wintertime:
534 Results from high resolution aerosol mass spectrometry, Journal of Geophysical Research-Atmospheres, 117, 2012a.

535 Ge, X. L., Zhang, Q., Sun, Y. L., Ruehl, C. R., and Setyan, A.: Effect of aqueous-phase processing on aerosol chemistry and size
536 distributions in Fresno, California, during wintertime, Environmental Chemistry, 9, 221-235, 2012b.

537 Grieshop, A. P., Donahue, N. M., and Robinson, A. L.: Laboratory investigation of photochemical oxidation of organic aerosol
538 from wood fires 2: analysis of aerosol mass spectrometer data, Atmos. Chem. Phys., 9, 2227-2240, 2009.

539 Hallar, A. G., Petersen, R., Andrews, E., Michalsky, J., McCubbin, I. B., and Ogren, J. A.: Contributions of dust and biomass
540 burning to aerosols at a Colorado mountain-top site, Atmos. Chem. Phys., 15, 13665-13679, 2015.

541 Hennigan, C. J., Miracolo, M. A., Engelhart, G. J., May, A. A., Presto, A. A., Lee, T., Sullivan, A. P., McMeeking, G. R., Coe,
542 H., Wold, C. E., Hao, W. M., Gilman, J. B., Kuster, W. C., de Gouw, J., Schichtel, B. A., Collett, J. L., Kreidenweis, S. M., and
543 Robinson, A. L.: Chemical and physical transformations of organic aerosol from the photo-oxidation of open biomass burning
544 emissions in an environmental chamber, Atmospheric Chemistry and Physics, 11, 7669-7686, 2011.

545 Heringa, M. F., DeCarlo, P. F., Chirico, R., Tritscher, T., Dommen, J., Weingartner, E., Richter, R., Wehrle, G., Prévôt, A. S. H.,
546 and Baltensperger, U.: Investigations of primary and secondary particulate matter of different wood combustion appliances with a
547 high-resolution time-of-flight aerosol mass spectrometer, Atmos. Chem. Phys., 11, 5945-5957, 2011.

548 Huffman, J. A., Docherty, K. S., Aiken, A. C., Cubison, M. J., Ulbrich, I. M., DeCarlo, P. F., Sueper, D., Jayne, J. T., Worsnop,
549 D. R., Ziemann, P. J., and Jimenez, J. L.: Chemically-resolved aerosol volatility measurements from two megacity field studies,
550 Atmospheric Chemistry and Physics, 9, 7161-7182, 2009.

551 IPCC: IPCC - Climate Change 2013: The Physical Science Basis, 2013. 2013.

552 Jaffe, D., Hafner, W., Chand, D., Westerling, A., and Spracklen, D.: Interannual Variations in PM2.5 due to Wildfires in the
553 Western United States, Environmental Science & Technology, 42, 2812-2818, 2008.

554 Jaffe, D. A. and Wigder, N. L.: Ozone production from wildfires: A critical review, Atmospheric Environment, 51, 1-10, 2012.

555 Jolleys, M. D., Coe, H., McFiggans, G., Taylor, J. W., O'Shea, S. J., Le Breton, M., Bauguitte, S. J. B., Moller, S., Di Carlo, P.,
556 Aruffo, E., Palmer, P. I., Lee, J. D., Percival, C. J., and Gallagher, M. W.: Properties and evolution of biomass burning organic
557 aerosol from Canadian boreal forest fires, Atmos. Chem. Phys., 15, 3077-3095, 2015.

558 Kondo, Y., Matsui, H., Moteki, N., Sahu, L., Takegawa, N., Kajino, M., Zhao, Y., Cubison, M. J., Jimenez, J. L., Vay, S., Diskin,
559 G. S., Anderson, B., Wisthaler, A., Mikoviny, T., Fuelberg, H. E., Blake, D. R., Huey, G., Weinheimer, A. J., Knapp, D. J., and

Atmospheric
Chemistry
and Physics
Discussions

Open Access

EGU

560   Brune, W. H.: Emissions of black carbon, organic, and inorganic aerosols from biomass burning in North America and Asia in
561   2008, Journal of Geophysical Research: Atmospheres, 116, D08204, 2011.

562   Kroll, J. H., Donahue, N. M., Jimenez, J. L., Kessler, S. H., Canagaratna, M. R., Wilson, K. R., Altieri, K. E., Mazzoleni, L. R.,
563   Wozniak, A. S., Bluhm, H., Mysak, E. R., Smith, J. D., Kolb, C. E., and Worsnop, D. R.: Carbon oxidation state as a metric for
564   describing the chemistry of atmospheric organic aerosol, Nature Chemistry, 3, 133-139, 2011.

565   Lee, A. K. Y., Willis, M. D., Healy, R. M., Wang, J. M., Jeong, C. H., Wenger, J. C., Evans, G. J., and Abbatt, J. P. D.: Single-
566   particle characterization of biomass burning organic aerosol (BBOA): evidence for non-uniform mixing of high molecular weight
567   organics and potassium, Atmos. Chem. Phys., 16, 5561-5572, 2016.

568   Lewis, K. A., Arnott, W. P., Moosmüller, H., Chakrabarty, R. K., Carrico, C. M., Kreidenweis, S. M., Day, D. E., Malm, W. C.,
569   Laskin, A., Jimenez, J. L., Ulbrich, I. M., Huffman, J. A., Onasch, T. B., Trimborn, A., Liu, L., and Mishchenko, M. I.:
570   Reduction in biomass burning aerosol light absorption upon humidification: roles of inorganically-induced hygroscopicity,
571   particle collapse, and photoacoustic heat and mass transfer, Atmos. Chem. Phys., 9, 8949-8966, 2009.

572   Liu, Y., Goodrick, S., and Heilman, W.: Wildland fire emissions, carbon, and climate: Wildfire–climate interactions, Forest
573   Ecology and Management, 317, 80-96, 2014.

574   Maudlin, L. C., Wang, Z., Jonsson, H. H., and Sorooshian, A.: Impact of wildfires on size-resolved aerosol composition at a
575   coastal California site, Atmospheric Environment, 119, 59-68, 2015.

576   May, A. A., Levin, E. J. T., Hennigan, C. J., Riipinen, I., Lee, T., Collett, J. L., Jimenez, J. L., Kreidenweis, S. M., and Robinson,
577   A. L.: Gas-particle partitioning of primary organic aerosol emissions: 3. Biomass burning, Journal of Geophysical Research:
578   Atmospheres, 118, 2013JD020286, 2013.

579   May, A. A., Lee, T., McMeeking, G. R., Akagi, S., Sullivan, A. P., Urbanski, S., Yokelson, R. J., and Kreidenweis, S. M.:
580   Observations and analysis of organic aerosol evolution in some prescribed fire smoke plumes, Atmos. Chem. Phys., 15, 6323-
581   6335, 2015.

582   Middlebrook, A. M., Bahreini, R., Jimenez, J. L., and Canagaratna, M. R.: Evaluation of Composition-Dependent Collection
583   Efficiencies for the Aerodyne Aerosol Mass Spectrometer using Field Data, Aerosol Science and Technology, 46, 258-271, 2012.

584   Ortega, A. M., Day, D. A., Cubison, M. J., Brune, W. H., Bon, D., de Gouw, J. A., and Jimenez, J. L.: Secondary organic aerosol
585   formation and primary organic aerosol oxidation from biomass-burning smoke in a flow reactor during FLAME-3, Atmos. Chem.
586   Phys., 13, 11551-11571, 2013.

587   Paatero, P. and Tapper, U.: POSITIVE MATRIX FACTORIZATION - A NONNEGATIVE FACTOR MODEL WITH
588   OPTIMAL UTILIZATION OF ERROR-ESTIMATES OF DATA VALUES, Environmetrics, 5, 111-126, 1994.

589   Paciga, A., Karnezi, E., Kostenidou, E., Hildebrandt, L., Psichoudaki, M., Engelhart, G. J., Lee, B. H., Crippa, M., Prévôt, A. S.
590   H., Baltensperger, U., and Pandis, S. N.: Volatility of organic aerosol and its components in the megacity of Paris, Atmos. Chem.
591   Phys., 16, 2013-2023, 2016.

Atmospheric
Chemistry
and Physics
Discussions

Open Access

EGU

592   Petters, M. D., Carrico, C. M., Kreidenweis, S. M., Prenni, A. J., DeMott, P. J., Collett, J. L., and Moosmüller, H.: Cloud
593   condensation nucleation activity of biomass burning aerosol, Journal of Geophysical Research: Atmospheres, 114, D22205, 2009.

594   Rinaldi, M., Gilardoni, S., Paglione, M., Sandrini, S., Fuzzi, S., Massoli, P., Bonasoni, P., Cristofanelli, P., Marinoni, A., Poluzzi,
595   V., and Decesari, S.: Organic aerosol evolution and transport observed at Mt. Cimone (2165 m a.s.l.), Italy, during the PEGASOS
596   campaign, Atmos. Chem. Phys., 15, 11327-11340, 2015.

597   Spracklen, D. V., Mickley, L. J., Logan, J. A., Hudman, R. C., Yevich, R., Flannigan, M. D., and Westerling, A. L.: Impacts of
598   climate change from 2000 to 2050 on wildfire activity and carbonaceous aerosol concentrations in the western United States,
599   Journal of Geophysical Research: Atmospheres, 114, D20301, 2009.

600   Sun, Y., Zhang, Q., Macdonald, A. M., Hayden, K., Li, S. M., Liggio, J., Liu, P. S. K., Anlauf, K. G., Leaitch, W. R., Steffen, A.,
601   Cubison, M., Worsnop, D. R., van Donkelaar, A., and Martin, R. V.: Size-resolved aerosol chemistry on Whistler Mountain,
602   Canada with a high-resolution aerosol mass spectrometer during INTEX-B, Atmos. Chem. Phys., 9, 3095-3111, 2009.

603   Sun, Y. L., Zhang, Q., Schwab, J. J., Yang, T., Ng, N. L., and Demerjian, K. L.: Factor analysis of combined organic and
604   inorganic aerosol mass spectra from high resolution aerosol mass spectrometer measurements, Atmospheric Chemistry and
605   Physics, 12, 8537-8551, 2012.

606   Timonen, H., Jaffe, D. A., Wigder, N., Hee, J., Gao, H., Pitzman, L., and Cary, R. A.: Sources of carbonaceous aerosol in the free
607   troposphere, Atmospheric Environment, 92, 146-153, 2014.

608   Ulbrich, I. M., Canagaratna, M. R., Zhang, Q., Worsnop, D. R., and Jimenez, J. L.: Interpretation of organic components from
609   Positive Matrix Factorization of aerosol mass spectrometric data, Atmospheric Chemistry and Physics, 9, 2891-2918, 2009.

610   Weiss-Penzias, P., Jaffe, D. A., Swartzendruber, P., Dennison, J. B., Chand, D., Hafner, W., and Prestbo, E.: Observations of
611   Asian air pollution in the free troposphere at Mount Bachelor Observatory during the spring of 2004, Journal of Geophysical
612   Research: Atmospheres, 111, D10304, 2006.

613   Westerling, A. L., Hidalgo, H. G., Cayan, D. R., and Swetnam, T. W.: Warming and Earlier Spring Increase Western U.S. Forest
614   Wildfire Activity, Science, 313, 940-943, 2006.

615   Wigder, N. L., Jaffe, D. A., and Saketa, F. A.: Ozone and particulate matter enhancements from regional wildfires observed at
616   Mount Bachelor during 2004–2011, Atmospheric Environment, 75, 24-31, 2013.

617   Yokelson, R. J., Crounse, J. D., DeCarlo, P. F., Karl, T., Urbanski, S., Atlas, E., Campos, T., Shinozuka, Y., Kapustin, V., Clarke,
618   A. D., Weinheimer, A., Knapp, D. J., Montzka, D. D., Holloway, J., Weibring, P., Flocke, F., Zheng, W., Toohey, D., Wennberg,
619   P. O., Wiedinmyer, C., Mauldin, L., Fried, A., Richter, D., Walega, J., Jimenez, J. L., Adachi, K., Buseck, P. R., Hall, S. R., and
620   Shetter, R.: Emissions from biomass burning in the Yucatan, Atmos. Chem. Phys., 9, 5785-5812, 2009.

621   Young, D. E., Kim, H., Parworth, C., Zhou, S., Zhang, X., Cappa, C. D., Seco, R., Kim, S., and Zhang, Q.: Influences of
622   emission sources and meteorology on aerosol chemistry in a polluted urban environment: results from DISCOVER-AQ
623   California, Atmos. Chem. Phys., 16, 5427-5451, 2016.

624 Yu, L., Smith, J., Laskin, A., George, K. M., Anastasio, C., Laskin, J., Dillner, A. M., and Zhang, Q.: Molecular transformations
625 of phenolic SOA during photochemical aging in the aqueous phase: competition among oligomerization, functionalization, and
626 fragmentation, Atmos. Chem. Phys., 16, 4511-4527, 2016.

627 Zauscher, M. D., Wang, Y., Moore, M. J. K., Gaston, C. J., and Prather, K. A.: Air Quality Impact and Physicochemical Aging of
628 Biomass Burning Aerosols during the 2007 San Diego Wildfires, Environmental Science & Technology, 47, 7633-7643, 2013.

629 Zhang, Q., Canagaratna, M. R., Jayne, J. T., Worsnop, D. R., and Jimenez, J. L.: Time- and size-resolved chemical composition
630 of submicron particles in Pittsburgh: Implications for aerosol sources and processes, Journal of Geophysical Research-
631 Atmospheres, 110, 19, 2005.

632 Zhang, Q., Jimenez, J. L., Canagaratna, M. R., Ulbrich, I. M., Ng, N. L., Worsnop, D. R., and Sun, Y. L.: Understanding
633 atmospheric organic aerosols via factor analysis of aerosol mass spectrometry: a review, Anal. Bioanal. Chem., 401, 3045-3067,
634 2011.

635 Zhou, S., Collier, S., Xu, J., Mei, F., Wang, J., Lee, Y.-N., Sedlacek, A. J., Springston, S. R., Sun, Y., and Zhang, Q.: Influences
636 of upwind emission sources and atmospheric processing on aerosol chemistry and properties at a rural location in the
637 Northeastern U.S, Journal of Geophysical Research: Atmospheres, doi: 10.1002/2015JD024568, 2016. 2015JD024568, 2016.

638

639
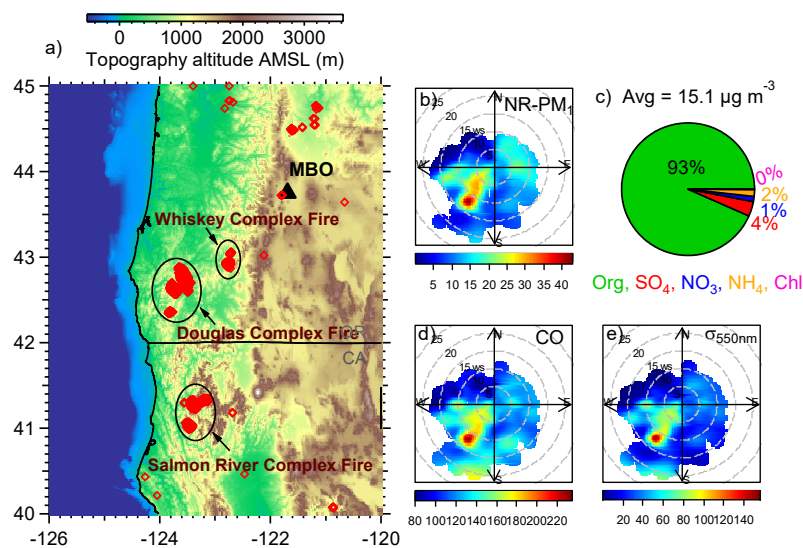
Fig. 1. a) Map with MBO (black solid triangle) and wildfires detected by MODIS (red open diamonds) in the Northwest Pacific US from July 25 to August 25, 2013. Three fire complexes, Whiskey Complex Fire (WCF), Douglas Complex Fire (DCF), and Salmon River Complex Fire (SRCF) are highlighted with black circles. Bivariate polar plots of (b) NR-PM$_1$ concentrations (in µg m^{-3}), d) submicrometer aerosol light scattering at 550 nm (σ_{550nm} in Mm^{-1}) and (e) CO mixing ratio (in ppbv) during the sampling period. c) Average NR-PM$_1$ composition for the sampling period.

646
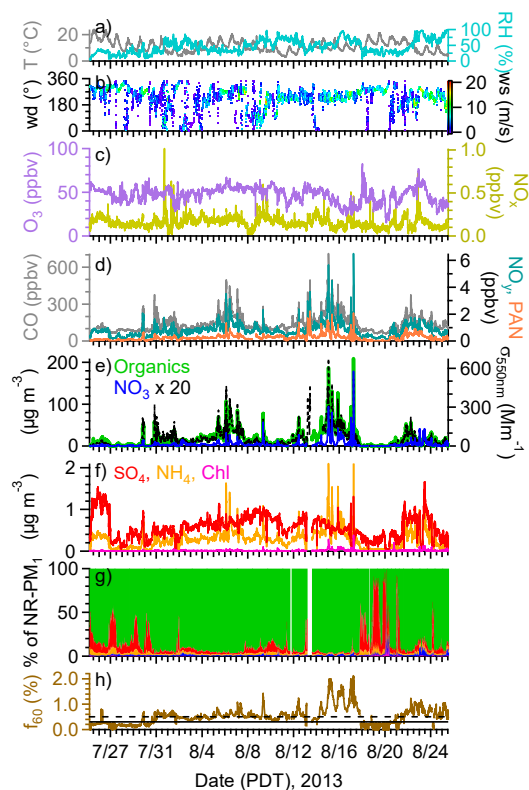
Fig. 2. Time series of (a) temperature (T) and relative humidity (RH), (b) wind direction (WD) colored by wind
speed (WS), (c) mixing ratios of O_3 and NO_x, (d) mixing ratios of CO, NO_y and PAN, (e and f) mass concentrations
of NR-PM$_1$ species and σ_{550nm} in STP (T = 273 K, P = 1013.25 hPa), (g) NR-PM$_1$ composition, and (h) f_{60} (=
$C_2H_4O_2^+$ / OA). The solid and broken lines in (h) indicate f_{60} = 0.3% and f_{60} = 0.5%, respectively.

Atmospheric
Chemistry
and Physics
Discussions

Open Access

EGU

651
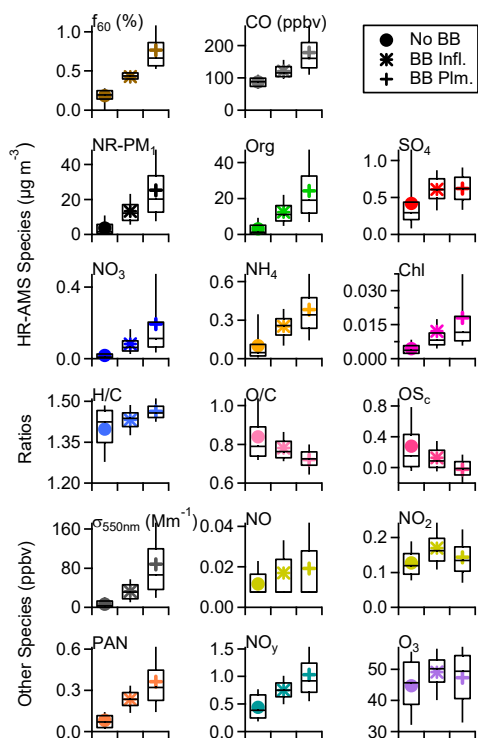
Fig. 3. Box plots that compare f_{60} values, CO mixing ratios, NR-PM$_1$ species concentrations, OA elemental ratios,
carbon oxidation states (OS$_c$), σ_{550nm}, and mixing ratios of trace gases among three aerosol regimes ("No BB", "BB
Infl", and "BB Plm"). The whiskers indicate the 90th and 10th percentiles, the upper and lower boundaries indicate
the 75th and 25th percentiles, and the lines in the boxes indicate the median values and the markers indicate the mean
values.

Atmospheric
Chemistry
and Physics
Discussions
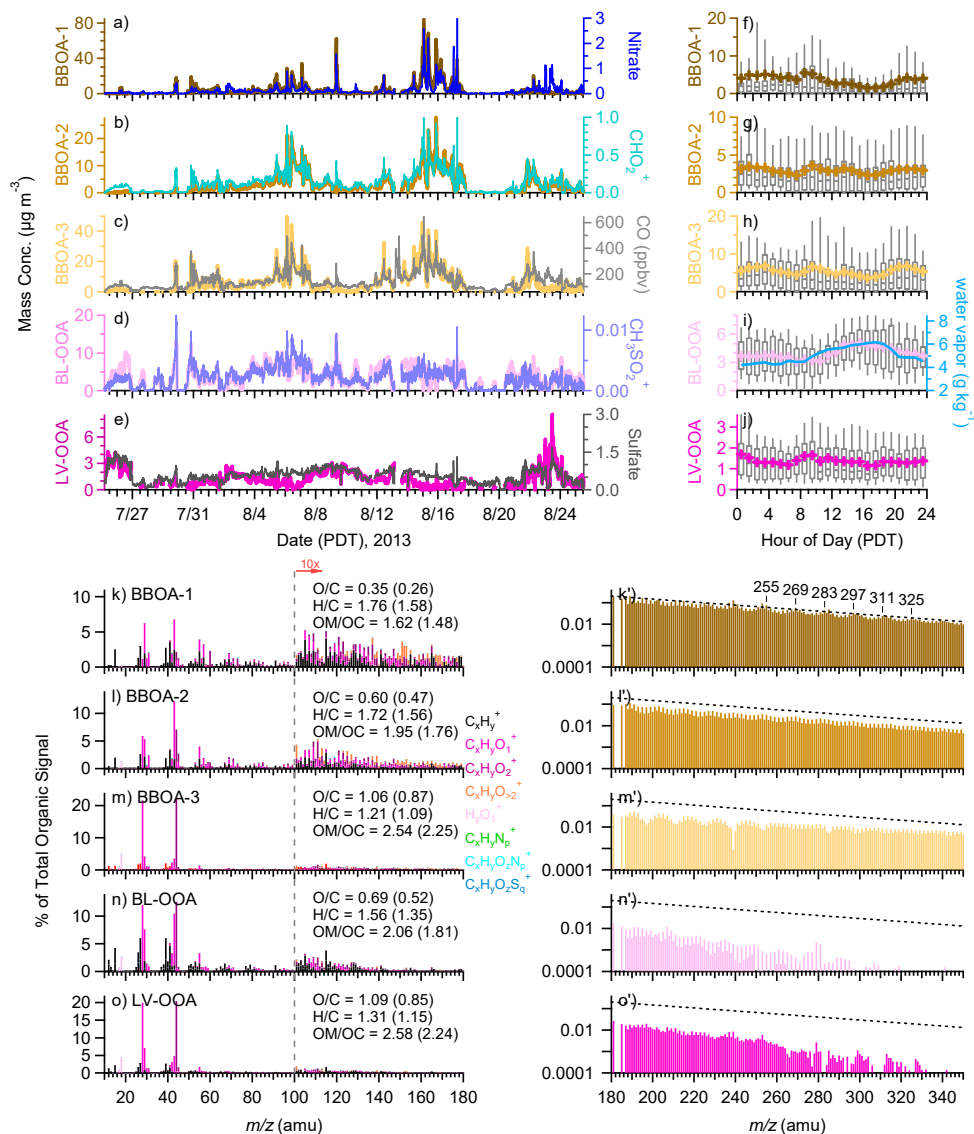
**Fig. 4.** (a-e) Time series of OA factors and corresponding tracer compounds. Organic ions are in organic equivalent mass; (f-g) Diurnal variations of OA factors (the whiskers above and below the boxes indicate the 90th and 10th percentiles, the upper and lower boundaries indicate the 75th and 25th percentiles, and the lines in the boxes indicate the median values and the cross symbols indicate the mean values) with the diurnal cycle of mean water vapor in (i); (k-o) HRMS of OA factors colored by eight ion families at $m/z < 180$ and (k'-o') UMR MS at $m/z > 180$ for each OA factor. The elemental ratios of each OA factor are shown in the legends of (k-o) with those obtained using the AA method in parenthesis.

Atmospheric
Chemistry
and Physics

Open Access

EGU

Discussions

665
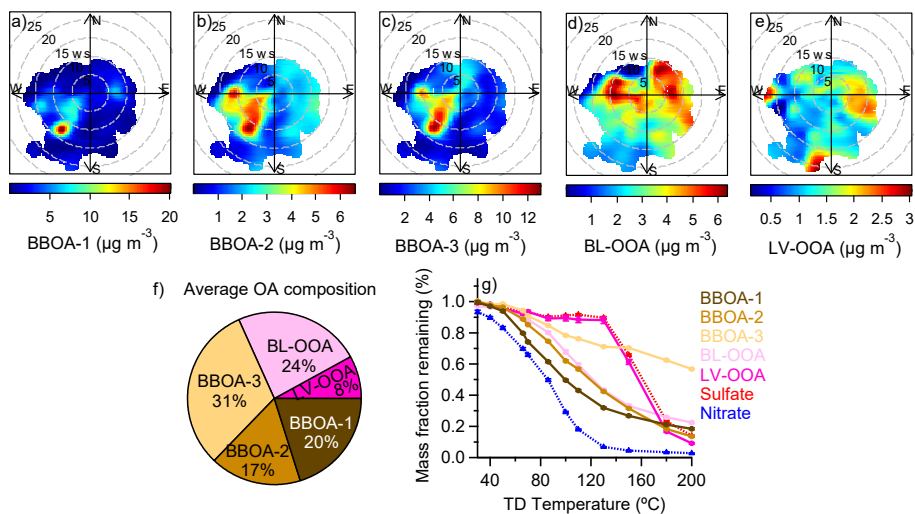
Fig. 5. (a-e) Bivariate polar plots that illustrate the variations of the concentrations of each OA factor as a

function of wind speed (m s^{-1}) and wind direction; (f) Average OA composition during the sampling period; (g)

Volatility profiles of OA factors, sulfate, and nitrate.

Atmospheric
Chemistry
and Physics
Discussions

669
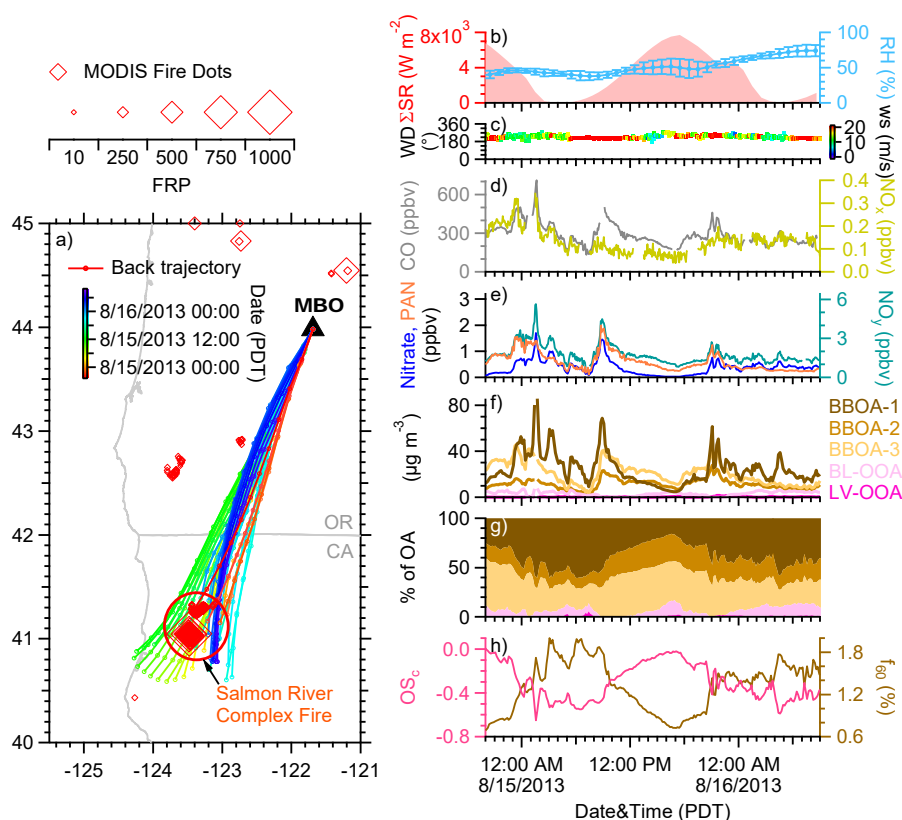
Fig. 6. (a) Map of the Pacific Northwest with the location of MBO marked by black triangle. Open diamonds represent MODIS satellite fire dots detected during August 13 – 17, 2013, and are sized by fire radiative power (FRP). Twelve-hour HYSPLIT back trajectories of air masses arriving at MBO from August 14 20:00 to August 16 09:00 are colored by time of arrival at MBO. Markers indicate 1-hour interval; (b) Cumulative solar radiation ($\sum$SR) and average RH for each trajectory; (c) Wind direction (WD) colored by wind speed (WS) measured at MBO; Mixing ratios of (d) CO, NO_x, (e) nitrate, PAN, and NO_y; (f) Five OA factors; (g) OA composition; (h) Average carbon oxidation states and f_{60} of OA during the Salmon River Complex Fire (SRCF) case study period.
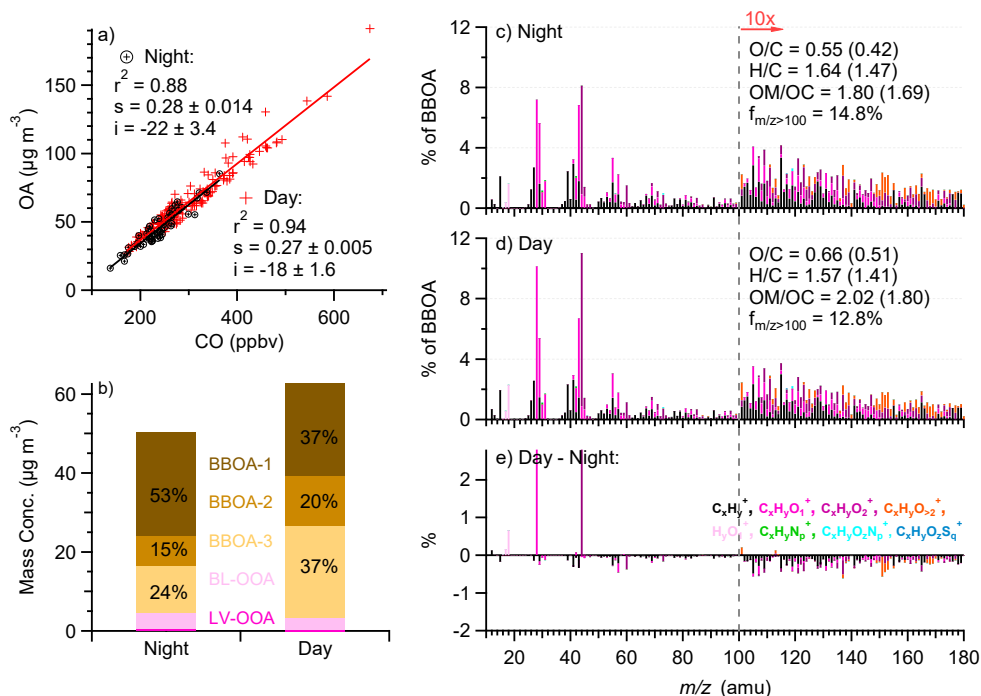
Atmospheric
Chemistry
and Physics
Discussions

Open Access

EGU

677
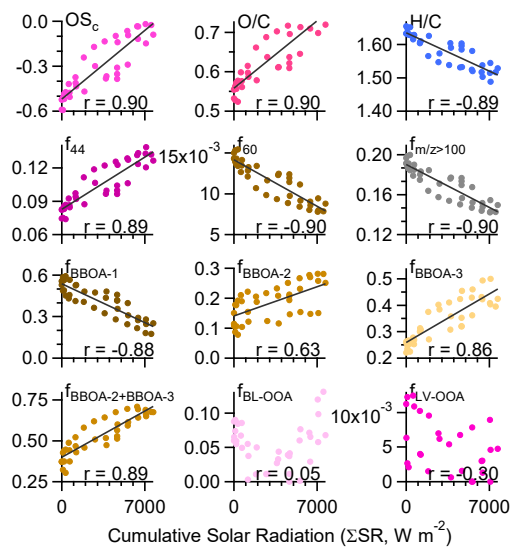
Fig. 7. Aerosol chemistry parameters of total BBOA as a function of cumulative solar radiation for the Salmon

River Complex Fire case study. The Pearson's correlation coefficients (r) are reported.

680

681   **Fig. 8.** (a) OA vs. CO during August 14 20:00 to August 16 09:00 with night-time transported plumes illustrated

682   as black circles and day-time transported plumes as red crosses. The orthogonal distance regression (ODR) results

683   for the two plume types are shown with the 1-σ uncertainties reported for the fit slopes (s) and intercepts (i); (b) A

684   comparison of the average concentrations of 5 OA factors (stacked) between the night-time and day-time transported

685   plumes. The average mass fractions of the BBOAs to total OA mass in each plume type are reported; (c) Average

686   HRMS of total BBOA for the night-time transported plumes; (d) Average HRMS of total BBOA for the day-time

687   transported plumes and (e) Difference BBOA HRMS between day and night plumes. The elemental ratios of BBOA

688   calculated with the IA method are shown in the legends of (c) and (d) with those obtained using the AA method in

689   parenthesis.